JOURNAL OF APPLIED PHYSICS VOLUME 88, NUMBER 3 1 AUGUST 2000

Edge-emission electroluminescence study of as-grown vertical-cavity surface-emitting laser structures

Sandip Ghosh, Stephanie Constant, Thomas J. C. Hosea,[a]
and T. E. Sale
Department of Physics, University of Surrey, Guildford GU2 5XH, United Kingdom

(Received 22 February 2000; accepted for publication 22 April 2000)

We report polarized edge- and front-emission electroluminescence studies on red-emitting vertical-cavity surface-emitting laser (VCSEL) structures. The measurements were performed nondestructively on pieces of as-grown wafers using indium–tin–oxide-coated glass electrodes. The front-emission spectra helped determine the Fabry–Pérot cavity-mode wavelength, while the edge-emission spectra were used to identify the wavelength of ground-state emission from the quantum wells (QWs) in the active region. However, measurements on edge-emitting laser (EEL) structures with a similar QW active region reveal that the peaks of the edge-emission spectra are always slightly redshifted with respect to front emission. We show that this arises due to reabsorption effects and then appropriately correct for it in the VCSELs by studying such shifts in the equivalent EELs. Thereafter, by comparing the experimental results with theoretical calculations and simulations, we estimate the composition, strain, and material quality of the QWs in the VCSEL active regions. Finally, we comment on the usefulness of comparing the two orthogonally polarized edge-emission spectra. © *2000 American Institute of Physics.* [S0021-8979(00)01715-1]

I. INTRODUCTION

Interest in vertical-cavity surface-emitting lasers (VCSELs) has increased in recent years since they have several advantages, such as single-longitudinal-mode operation, symmetric beam profile, low beam divergence, low threshold currents, low temperature sensitivity of emission wavelengths, ease of integration into two-dimensional arrays, and on wafer testability.[1,2] Of crucial importance to the working of a VCSEL is the relative wavelengths of the single longitudinal Fabry–Pérot cavity mode and the peak of the gain spectrum of the quantum well (QW) in the active region. The extent to which these features are in resonance strongly influences the threshold current density and the power output, and their temperature dependence.[3–5] VCSEL structures are designed such that, at room temperature, the gain peak is at a shorter wavelength than that of the cavity mode and, as the operating device warms up due to Ohmic heating from the drive current, the peak of the gain redshifts and comes into resonance with the cavity mode (which is much less temperature sensitive). However, the cavity-mode wavelength and band over which the distributed Bragg reflectors (DBRs) have high reflectivity depend critically on the thickness of the layers. An error of say 1% in the growth rate of all the layers would shift the device operating wavelength by $\simeq 1\%$, i.e., by 6.5 nm for a 650 nm design, which may be very significant if the system specifications are tight. Furthermore, in red VCSELs with an AlGaInP-based cavity, it is difficult to grow the cavity to the correct length such that the cavity mode is centered on the high-reflectivity band of the DBRs, thereby affecting the minimum achievable threshold gain. While both these dimensional factors can lead to significant variation in the cavity-mode wavelength, a compositional change will affect mainly the QW emission wavelengths. Thus, an important aspect of postgrowth characterization of VCSEL structures is to determine the relative wavelengths of the peak of the QW emission and the cavity mode.

While it is relatively easy to determine the position of the cavity mode using reflectance measurements,[6] nondestructive estimation of the QW emission peak is difficult because measurements through the front surface are strongly modified by the presence of the DBRs. To observe photoluminescence (PL) from the QW, the front DBR is often etched away,[7] but this is obviously destructive and such PL can still be modified by the bottom DBR stack. Front surface photoreflectance has been shown to be more useful,[8–10] but it works best when the top DBR reflectivity is not too high and the inhomogenous broadening of the critical-point energies is relatively small. However, the in-plane QW emission spectrum from regions close to the edge of a VCSEL is expected to be largely free of the effects of the DBRs and would, therefore, be more useful in identifying the QW emission peak. PL spectra measured in this geometry have been reported by Schaafsma and Christensen[11] and Gramlich *et al.*,[12] which we will discuss subsequently in relation to our observations. Here, we report polarized edge-emission electroluminescence (EL) studies on as-grown VCSEL structures emitting in the red. First, we briefly describe the samples and our nondestructive EL technique. Then, using edge-emitting laser (EEL) structures, we show that the peaks of the edge-emission EL spectra are always slightly redshifted. We use a model to show why this occurs and go on to describe how to correct for this shift in VCSELs. Thereafter, comparing the experimental results with theoretical calculations, we explain some of the observed experimental trends and estimate the

[a]Electronic mail: j.hosea@surrey.ac.uk

 © 2000 American Institute of Physics

Downloaded 02 Sep 2003 to 158.144.58.158. Redistribution subject to AIP license or copyright, see http://ojps.aip.org/japo/japcr.jsp

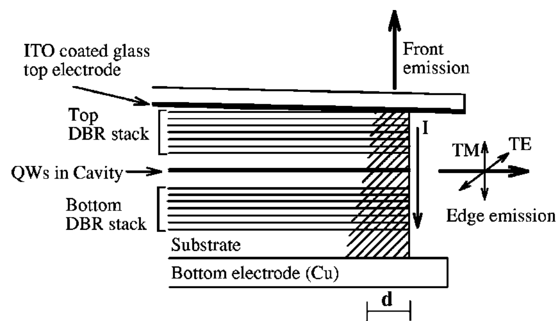

FIG. 1. Schematic of the electroluminescence (EL) emission geometry, the shaded portion indicating the dominant current (I) path, of approximate thickness d (not drawn to scale).

composition and strain in the QW active region of these VCSELs. Finally, we discuss the usefulness, in terms of VCSEL characterization, of comparing the two orthogonally polarized edge-emission spectra.

II. EXPERIMENT

The VCSEL samples studied here were grown by metal–organic chemical-vapor deposition, with active regions comprising four $Ga_xIn_{1-x}P/(Al_{0.3}Ga_{0.7})_{0.52}In_{0.48}P$ QWs, with well and barrier widths of $L_w = 45$ Å and $L_b = 50$ Å, respectively. The QWs were in a Fabry–Pérot cavity layer made of $(Al_{0.7}Ga_{0.3})_{0.52}In_{0.48}P$, sandwiched between two p^+- and n^+-doped DBR stacks, comprising several pairs of $Al_{y1}Ga_{1-y1}As/Al_{y2}Ga_{1-y2}As$ layers. The structures were grown on n^+-GaAs(100) substrates miscut 10° towards ⟨111⟩, in order to prevent ordering in the $Ga_xIn_{1-x}P$ layers. The five VCSEL structures studied (labeled V1–V5) were designed for different emission wavelengths in the red region of the spectrum and differ in terms of the Ga concentration in the QWs and Al concentration in the DBRs. Also studied were a set of EEL structures (labeled E1–E5) which had QW active regions and cladding similar to the corresponding VCSELs V1–V5, but with the DBR stacks replaced by thick $Al_yGa_{1-y}As$ layers.

The EL measurements were performed using an arrangement shown schematically in Fig. 1. The as-grown samples, cleaved into 5 mm×5 mm square pieces, were placed between two electrodes, the bottom one a grounded copper plate, and the top a transparent conducting (20 Ω per square) indium–tin–oxide (ITO) -coated glass slide. The top electrode was pressed down lightly on the sample at a slight angle such that it preferentially touched along one edge. As a result, the current was confined close to this edge so that light was generated in a strip of the the active region 5 mm long and of width $\sim d$, along this edge of the sample. The EL was excited with a positive square-wave voltage and resultant currents were, typically, <15 mA. The average width of the strip over which light was generated was estimated to be $d \simeq 30$ μm. Thus, the current densities involved were around 10 A cm^{-2}, which were too small to cause any damage to the sample. The arrangement allowed us to detect EL emerging from both the front and edge of the sample. Other details about the experimental arrangement can be found in Ref. 14. Using polymer sheet polarizers, the edge-emission spectra were measured in the transverse magnetic (TM) and transverse electric (TE) polarizations. In the first case, the electric vector is perpendicular to the plane of the QW and in the second, parallel to it. The EL was dispersed by a 0.32 m monochromator and detected with a Si photodiode and lock-in amplifier combination. The front-emission spectra, emerging through the DBRs, had narrow spectral features due to the effect of the optical cavity, so these were recorded with a bandpass of $\simeq$0.15 nm. The weaker edge-emission spectra were much broader, typically, larger than 17 nm, and therefore, larger slit widths corresponding to a bandpass of, typically, 4 nm, could be used. In edge emission the light collection cone was kept small ($\simeq$7°) to avoid detecting scattered front-emission light. All spectra were recorded at room temperature, and were corrected for the wavelength response of the system.

Before ending this section we note that although PL can, in principle, give similar information about the active region of a laser structure, our nondestructive EL technique has some advantages. PL often requires cooling to get sufficiently strong signals. In an EL measurement the active region is selectively excited and, therefore, the QW emission is easily identified, while in PL the interpretation of the spectra may be complicated by emissions from various other layers. More specifically, in the case of PL measurements on VCSELs, if the pump laser wavelength is close to the high-reflectance band of the DBRs, it is virtually completely reflected. On the other hand, if it is at a much shorter wavelength it gets strongly absorbed in the top DBR layers, making it difficult to measure sufficient PL signal from the active region. Thus, pump lasers operating at different wavelengths would be required for PL experiments on different VCSEL structures. Also, with the present arrangement we were able to detect sufficient EL coming out of the edge of the sample (which is of crucial importance to this study) with greater ease than is possible in a typical PL experiment in this geometry.

III. RESULTS AND DISCUSSION

Figure 2 shows the normal-incidence reflectivity (R) of a typical VCSEL sample, together with the front emission, and two orthogonally polarized edge-emission EL spectra. The small dip in the R spectrum at 661 nm identifies the position of the Fabry–Pérot cavity mode. In the front-emission EL spectrum we get a much better defined feature at the cavity-mode wavelength and also several other features at positions corresponding to dips in the R spectrum. This EL spectrum shows that the DBRs dramatically modify the light emitted from the front of the sample. Although such EL helps to identify the cavity-mode position accurately, it gives little clue as to the peak position of the QW emission. In contrast, the edge-emission spectra shown at the bottom of Fig. 2 are not affected by the DBRs. Though the edge emission from a VCSEL structure may be affected by the étalon filtering effect, whereby intensities at those frequencies favored in front surface emission are reduced in the edge emission, this effect is usually quite small.[11] This is confirmed here by the fact that we do not see any sharp dips in the edge-emission spec-

Downloaded 02 Sep 2003 to 158.144.58.158. Redistribution subject to AIP license or copyright, see http://ojps.aip.org/japo/japcr.jsp

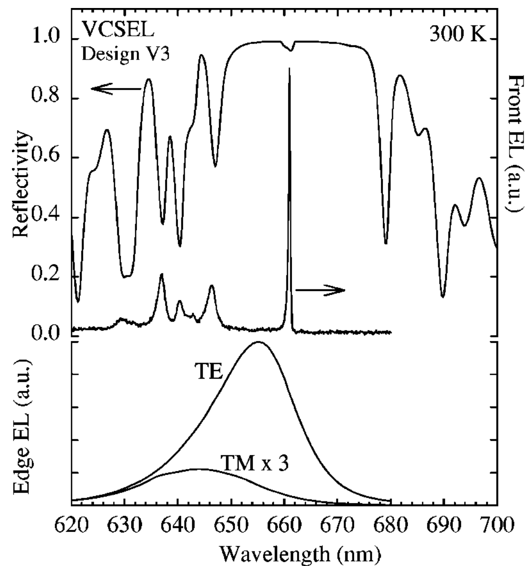

FIG. 2. Measured normal-incidence reflectivity, front and polarized (TE and TM) edge-emission EL from an as-grown vertical-cavity surface-emitting laser (VCSEL) structure.

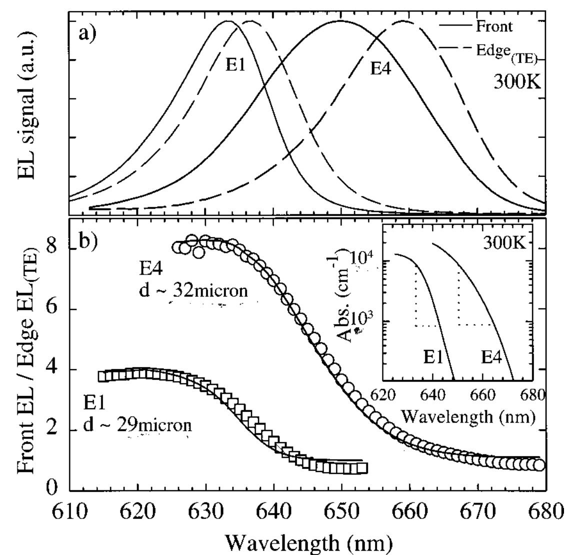

FIG. 3. (a) Measured front- and edge- (TE) emission EL spectra of two edge-emitting laser (EEL) structures (E1 and E4) with different Ga concentration in their QW active regions. The spectra are normalized to identical peak heights. (b) (circles and squares). The ratio of front- and edge- (TE) emission spectra of the two EELs. The ratios have been scaled by a constant so that the long-wavelength asymptote is unity. The lines represent best fits using Eq. (3) with $\beta=1$, $\Gamma=0.1$, and d values indicated. The inset shows the wavelength dependence of the absorption coefficient of the active regions of these two EELs determined from their front-emission spectra. The dotted lines show that E4 has the more broadened sub-band-gap absorption.

tra. Thus, these spectra are very useful in determining the true QW emission peak position. We note here that we see none of the additional interference-related structures seen in the edge-emission PL reported by Gramlich *et al.*[12] because, in their case, the pump laser excited all the different layers in the structure, while here, light is generated only in QWs in the active region defined by the $p-n$ junction. Also, unlike Schaafsma and Christensen[11] we do not see any Rabi splitting in the edge emission because the QW emission linewidths are much larger than the width of the cavity mode.[13] Of the two orthogonal polarizations of the edge-emission spectra, the TE polarization is relevant to the front-emission geometry and is, therefore, of importance to the working of a VCSEL. However, it would be too simplistic to take the peak of the edge TE emission as the true spontaneous TE emission peak position. This can be understood from a study of the corresponding EEL structures, as described next.

A. Peak shifts in edge emission

Figure 3(a) shows the front- and edge- (TE) emission spectra of two EEL structures, showing that, in both cases, the peak of the edge-emission spectrum is redshifted with respect to that of the front emission. In an electrically pumped EEL structure one can expect gain-related redshifts in the emission spectrum peak. However, this happens at much higher current densities [typically, $>250\ \mathrm{A\,cm^{-2}}$ (Ref. 15)], than here (typically, $10\ \mathrm{A\,cm^{-2}}$). Second, the width of a gain-related feature in an emission spectrum increases significantly with increase in carrier density, but we saw no appreciable change in the width of the edge-emission spectra, even when the current was increased tenfold. These observations indicate that this redshift in the peak of the edge-emission spectra is not due to optical gain. We suggest that the shift can be understood by considering reabsorption effects, as follows. Photons generated at a distance from the edge of the sample, and traveling in the plane of the QW, have to pass through an absorbing medium (the rest of the QW) before they emerge from the sample edge. Since the absorption coefficient drops with increasing wavelength, long-wavelength photons are thus more likely to survive to exit the edge of the structure and be detected, thereby shifting the emission peak to longer wavelengths. In the front-emission geometry any redshift would be negligible by comparison, because the maximum distance over which absorption occurs is of the order of the thickness of the QW, which is negligible compared to that in edge emission. These spectral shifts can be modeled as follows.

We assume that the sample is uniformly pumped in the QW active layer up to an average distance d from the edge of the sample as shown in Fig. 1. If $g_0(\lambda)$ is the consequent uniform rate of generation light per unit volume, then, using an analysis similar to that of Henry *et al.*,[16] the total intensity of light emerging from the edge $I_E(\lambda)$, with the edge chosen to be at the origin, will be given by

$$I_E(\lambda)=A_E\int_{-d}^{0}(1-R)g_o(\lambda)e^{\Gamma\alpha(\lambda)x}dx$$

$$=\frac{A_E(1-R)g_o(\lambda)}{\Gamma\alpha(\lambda)}[1-e^{-\Gamma\alpha(\lambda)d}], \tag{1}$$

where $\alpha(\lambda)$ is the wavelength-dependent absorption coefficient in the active region, Γ the optical confinement factor (calculated to be 0.1 in these device structures), R the reflectivity at the air/active region interface, $A_E\simeq(4L_w+3L_b)l_s$ the average area in which light is generated, and l_s the length of the sample edge ($\simeq 5$ mm). Interference effects, due to reflection at the pumped/unpumped active region boundary,

Downloaded 02 Sep 2003 to 158.144.58.158. Redistribution subject to AIP license or copyright, see http://ojps.aip.org/japo/japcr.jsp

are neglected as the refractive-index difference here is inconsequential, and absorption is assumed to obliterate any reflections from the distant far edge of the sample. For an EEL structure with no DBRs the intensity of light emerging from the front surface $I_F(\lambda)$, would be given by an expression similar to Eq. (1), but with d replaced by $(4L_w+3L_b)$, if we assume: (i) no significant absorption in the barrier/overlayers; (ii) light propagating in the direction of the substrate is not reflected back in any significant amount and is completely absorbed by the substrate; and (iii) the major reflection suffered by the light propagating towards the front surface is at the air/$Al_yGa_{1-y}As$ interface and is of similar magnitude to that at the air/active region interface for edge emission. These assumptions are quite reasonable, given the values of the complex refractive indices of the substrate ($\simeq 3.8+0.18i$), QW active region ($\simeq 3.5+0.045i$), $(Al_{0.7}Ga_{0.3})_{0.52}In_{0.48}P(\simeq 3.2+10^{-4}i)$ and $Al_yGa_{1-y}As(\simeq 3.3+10^{-4}i)$ layers at 655 nm. For front emission, the exponential term in Eq. (1) may be expanded binomially and truncated to first order, since typically, $\Gamma\alpha(\lambda)(4L_w+3L_b)\ll 1$, to yield

$$I_F(\lambda)=A_F(1-R)g_0(\lambda)(4L_w+3L_b), \quad A_F\simeq dl_s. \tag{2}$$

Dividing Eq. (2) by Eq. (1) gives the ratio of front-to-edge-emission spectra:

$$\frac{I_F(\lambda)}{I_E(\lambda)}=\frac{\beta\Gamma\alpha(\lambda)d}{1-e^{-\Gamma\alpha(\lambda)d}}, \tag{3}$$

where β describes the ratio of light collection efficiencies of the front- and the edge-emission experiments, which differ due to experimental constraints. Ideally, β should be 1, and so Eq. (3) should have an asymptote of unity at long wavelengths, where α is small. Therefore, if the experimentally determined ratio $I_F(\lambda)/I_E(\lambda)$ is normalized such that its long-wavelength asymptote equals 1, then it should be possible to fit this with Eq. (3) using only one fitting parameter d (the average width of the pumped region), if $\alpha(\lambda)$ is known. Figure 3(b) shows this ratio for structures E1 and E4.

Using the relation between absorption and emission[16] in a semiconductor at an energy ϵ and temperature T,

$$I(\epsilon)\simeq\alpha(\epsilon)\epsilon^2 e^{-\epsilon/k_BT}, \tag{4}$$

we can use the EEL's front-emission spectrum to derive its $\alpha(\lambda)$ spectrum, to within a multiplicative constant. This constant can then be fixed by demanding that the value of the absorption coefficient at the effective band-edge position ($\simeq$the front EL peak position for a QW) should equal its theoretically expected value α_o. The inset of Fig. 3(b) shows $\alpha(\lambda)$ determined in this fashion for device structures E1 and E4 using a theoretically calculated value including excitonic contribution[17] of $\alpha_0=9\times10^3\ \mathrm{cm}^{-1}$. The curves in Fig. 3(b) show the resulting fit of Eq. (3) to the experimentally determined $I_F(\lambda)/I_E(\lambda)$. Evidently, the fits are very satisfactory, giving similar fitted values for $d\simeq 30\ \mu$m. This value of d obviously depends on the theoretically calculated α_0, but its order of magnitude is consistent with the width of the luminescent strip observed visually during the experiments. Thus, the above analysis confirms that the redshifts in the edge-emission spectra are indeed due to reabsorption effects.

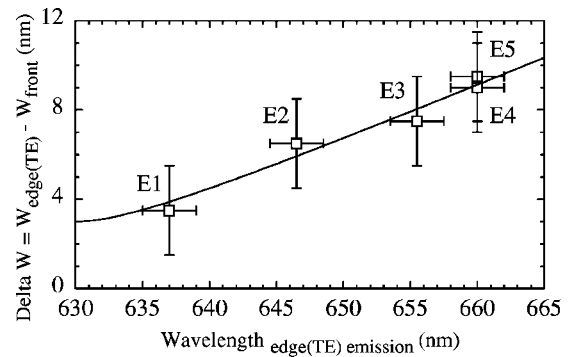

FIG. 4. (squares) Measured shift between the peak wavelength of the front- and edge- (TE) emission EL spectra of several EEL structures (with different Ga concentration in the QW active region) as a function of the edge- (TE) emission peak wavelength. The curve is a fit with the phenomenological relation given by Eq. (5).

Equation (3) indicates that the redshift of the edge-emission peak depends on the magnitude of d as well as the wavelength dependence and magnitude of $\alpha(\lambda)$, the latter two being sample dependent. This means that the measured edge (TE) peak positions would be unreliable if d changed significantly between different mountings. However, simulations of the reabsorption effect using Eq. (1), show that the redshifts are more sensitive to the λ dependence of $\alpha(\lambda)$, than to changes in the magnitude of d or $\alpha(\lambda)$. For instance, doubling d increases the redshift by only 2 nm but even a slight broadening of $\alpha(\lambda)$ in the sub-band-gap region results in much larger redshifts. This can be seen by comparing E1 and E4 in Fig. 3, where, in spite of the same d and α_o, the shift for E4 is much larger (6 nm) because of its more broadened sub-band-gap $\alpha(\lambda)$, as shown in the inset of Fig. 3(b). Furthermore, we observed that, between several remountings of the same sample, where one might expect d to change, the edge (TE) peak position was identical to within ± 2 nm. Additionally, there is a regular trend in the the five EEL structures studied, such that the redshift of the edge (TE) peak position (with respect to the front-emission peak) increases smoothly, as the peak positions themselves move towards longer wavelengths in going from E1 to E5. This is shown in Fig. 4 where the shift $\Delta\lambda=\lambda_{\mathrm{edge(TE)}}-\lambda_{\mathrm{front}}$ is plotted as a function of the edge (TE) peak position. An explanation for this trend will be suggested later, but note that it would not have occurred if the redshifts were dominated by arbitrary changes in d. Therefore, we are confident of the measured edge (TE) emission peak position to within $\simeq\pm 2$ nm. Our model shows that it is not possible to calculate the true spontaneous emission peak position from the edge-emission spectrum alone, unless d and $\alpha(\lambda)$ are known. Since there is no way of knowing these quantities *a priori* for VCSELs, we have adopted a different approach. We first fitted the following phenomenological expression to the peak shift data of the EELs in Fig. 4:

$$\Delta\lambda=3+\frac{a_1\lambda_r^2}{a_2+\lambda_r}, \quad \lambda_r=\lambda_{\mathrm{edge(TE)}}-630\ \ (\mathrm{nm}). \tag{5}$$

The above expression for $\Delta\lambda$ has a limiting value of 3 nm at $\lambda_{\mathrm{edge(TE)}}=630$ nm and was so chosen for reasons to be

Downloaded 02 Sep 2003 to 158.144.58.158. Redistribution subject to AIP license or copyright, see http://ojps.aip.org/japo/japcr.jsp

TABLE I. Values of relevant parameters of GaP, InP used in calculations to determine the theoretical optical transition wavelengths in the QW active region.

Parameter	GaP	InP
Lattice constant a_L (Å)	5.4505	5.8687
Spin-orbit splitting (eV)	0.08	0.108
Electron effective mass (m^*/m_0)	0.09	0.077
Luttinger parameter γ_1	4.05	5.04
Luttinger parameter γ_2	0.49	1.56
Hydrostatic deformation potential $a_{(\mathrm{VB+CB})}$ (eV)	−9.3	−6.4
Shear deformation potential $b_{(\mathrm{VB+CB})}$ (eV)	−1.6	−2.0
Elastic constant C_{11} (10^{11} dyn/cm^2)	14.1	10.1
Elastic constant C_{12} (10^{11} dyn/cm^2)	6.2	5.6

explained later. With the values of the fitted parameters $a_1 = 0.2505$ and $a_2 = 6.7614$ nm, this relation gives the expected redshift when the edge (TE) peak position is in the range 630–665 nm for these types of QWs. We then used this curve and the measured values of the edge- (TE) emission peak position in the VCSELs to work back to where their QW's front-emission peak position would have been.

B. Transition wavelengths: Theory and experiment

To analyze the experimental results further, we performed numerical calculations in the envelope-wave-function approximation using the transfer-matrix/tunneling-resonance technique,[18] in order to determine the allowed QW optical transition wavelengths. The calculations considered the well layers to be coherently strained with respect to the GaAs substrate (lattice constant = 5.563 Å).[19] The parameters of $Ga_xIn_{1-x}P$ used in the calculations were determined by appropriate linear interpolation between those for GaP and InP, taken from different sources,[15,19,20] and are listed in Table I. The band gap of the unstrained $Ga_xIn_{1-x}P$ random alloy in the well was taken to be $1.351 + 0.767x + 0.662x^2$ eV,[15] and that of the barrier $(Al_{0.3}Ga_{0.7})_{0.52}In_{0.48}P$ to be 2.1 eV,[15] while the conduction-/valence-band offset ratio chosen was 60/40.[21] The barrier effective masses used were $m_e^* = 0.11$, $m_{\mathrm{hh}}^* = 0.62$ and $m_{\mathrm{lh}}^* = 0.11$.[15]

Figure 5 shows the results of the calculation where only the low-energy heavy-hole and light-hole transitions relevant to the emission process have been shown. The lowest heavy- and light-hole energy levels are split into four because of the coupling between the four wells. The inset shows the simulated edge (TM and TE) and front-emission EL for $x_{\mathrm{Ga}} = 0.44$. The simulations were performed using Eq. (4), with a calculated $\alpha(\epsilon)$, which for a QW has a step-function-like energy dependence. Line broadening effects such as intraband relaxation and inhomogeneity were neglected. Notice that the peak of the front emission in the simulated spectra is not at the lowest-energy heavy-hole transition, but exactly at the fourth one. This is due to the product of the occupation probability with the near-band-edge absorption coefficient (consisting of four closely spaced steps, arising from the four split electron- and heavy-hole levels) becoming maximum at the fourth split heavy-hole transition. This effect is somewhat similar to the case of a three-dimensional (3D) M_0 critical point, where the front surface luminescence peak is

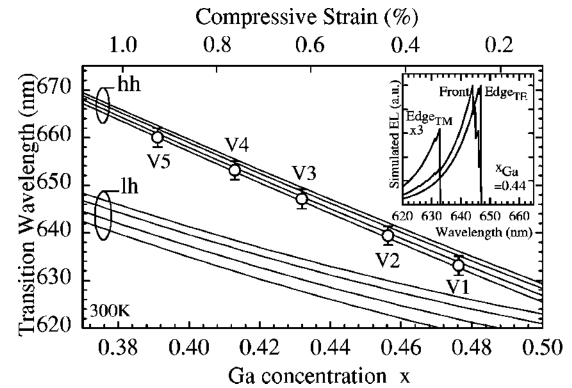

FIG. 5. Theoretically calculated transition wavelengths in the QW active regions of the VCSEL and EEL structures, as a function of Ga concentration (and strain). The circles are placed at points where the experimentally determined EL peak position of the VCSELs [i.e., edge- (TE) emission peak position, corrected for redshift] coincides with the theoretical peak position curve. The inset shows the simulated EL spectra for $x_{\mathrm{Ga}} = 0.44$ neglecting exciton, band tailing, Stark shift, and relaxation effects.

blueshifted by $\simeq k_B T/2$ away from the true band edge.[22] However, the simulated edge (TE) emission peak, which takes into account reabsorption through Eq. (3), is redshifted by $\simeq 3$ nm and exactly coincides with the lowest-energy heavy-hole transition. Therefore, this indicates that there will always be a redshift of at least $\simeq 3$ nm in these four coupled QW systems. This minimum possible redshift roughly corresponds to the splitting between the lowest and highest split heavy-hole transitions, which is almost independent of Ga concentration (Fig. 5). It also explains why we chose a limiting redshift of 3 nm in Eq. (5). The results in Fig. 5 also show that as the Ga concentration in the QW decreases, accompanied by increased compressive strain, the wavelength of the front-emission peak should move systematically to longer wavelengths.

The circles in Fig. 5 are placed at points where the measured peaks of the QW emission in the VCSELs [edge (TE) emission peaks, corrected for redshift using Eq. (5)], coincide with the calculated peak position, enabling the values of the Ga concentration and strain in the active region to be read off. The average concentration of Ga estimated thus ranged from 48% to 39% with an error of ±0.5%. Our simulations of the emission spectra also indicate that if broadened excitonic contributions are included, then the estimated Ga concentration would be higher than the above values by $\simeq 1\%$. These values are in agreement with the growers' independent estimate of the possible range of Ga concentrations in the QWs. Note that the transition wavelengths in a QW also depend on the well widths. However, the above estimates of Ga composition would be wrong by only ±1% even if the well widths differed by as much as ∓5 Å ($\simeq 11\%$). These results show that as the emission peaks shift to longer wavelengths from VCSEL V1 to V5, the strain in the QW layers also increases significantly, reaching a relatively high value of 0.9% ± 0.05% for sample V5. The four QWs in these structures are closely packed so the strain-thickness product is quite high. Since the devices made from these structures worked, we can conclude that strain is not significantly relieved through lattice dislocations as this

Downloaded 02 Sep 2003 to 158.144.58.158. Redistribution subject to AIP license or copyright, see http://ojps.aip.org/japo/japcr.jsp

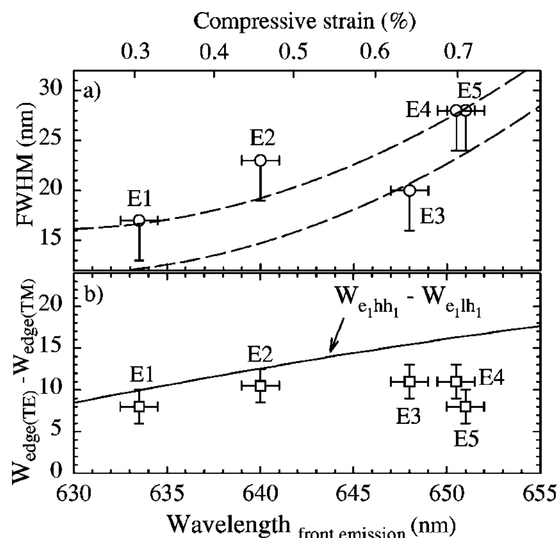

FIG. 6. (a) (circle) Measured full width at half maximum (FWHM) of the front EL emission spectra of the EELs (with different QW Ga concentrations), as a function of their front-emission peak wavelength. The dashed curves are a guide to the eye. The strain values (top axis) for a given peak wavelength were determined theoretically. (b) (squares) Measured difference between TE- and TM-polarized edge-emission EL peak wavelengths of the EELs, as a function of their front-emission peak wavelength. The curve represents the theoretically expected variation of the difference between the effective heavy- and light-hole band gaps.

would lead to very short device lifetimes. The strain field will affect the QW deposition during growth and it is likely that the upper QWs differ slightly from the lower ones and some degree of 3D growth or Ga–In segregation begins to occur. This inhomogeneity would result in broadening of the absorption edge which would increase as the strain increases. Consequently, one should expect relatively large emission linewidths. Figure 6(a) shows the full width at half maximum (FWHM) of the EEL's front-emission spectra, as a function of their front-emission peak wavelength. The FWHM estimated on the basis of the thermal distribution of carriers (see the inset of Fig. 5) was typically 8 nm, although this would be somewhat larger if carrier relaxation effects were included.[15] However, as seen in Fig. 6(a), the measured linewidths are in fact much larger than can be explained using these combined effects. Furthermore, the FWHMs tend to increase as the emission shifts to longer wavelengths, indicating that the absorption edge also broadens in going from E1 to E5. Since we showed earlier that increased broadening in the absorption spectrum leads to a larger redshift of the edge emission peaks, this also explains the observed increase in the redshift of the edge- (TE) emission peak, with respect to the front-emission peak, shown in Fig. 4. The increased inhomogeneous broadening of the QW absorption edge suggested that in the present set of VCSELS those that were designed to operate at the longer wavelengths would achieve less than their ideal efficiency. In a subsequent design, 665 nm QW emission was achieved by increasing the Ga concentration from the value of 0.38 indicated in Fig. 5, but using wider wells (80 Å). The resultant lower strain in this design led to a narrower QW emission linewidth (14 nm) as expected from the above arguments. This device (14 μm diam) lased at the cavity wavelength of 675 nm, with a peak output power of 2.5 mW at a current of 15 mA.

C. Importance of TM-polarized edge emission

In the simplest approximation, the edge- (TE) emission spectrum for a compressively strained QW is expected to be dominated by electron-to-heavy-hole transitions, while the edge-(TM) spectra will have contributions almost exclusively from light holes. The effective band-edge absorption is nearly the same for these two polarizations [i.e., $\alpha_o^{TM}(e1lh1) \simeq \alpha_o^{TE}(e1hh1)$],[23] so the positions of both peaks are expected to be redshifted by similar amounts, thereby preserving their difference. Since the difference between the heavy-hole and the light-hole effective-energy gaps can be an independent estimate of the composition and strain in the QW (as can be seen from Fig. 5), it should be possible to determine these parameters directly from the difference in the peak positions of the TE- and TM-polarized edge emissions of a VCSEL sample. However, in the present case this did not work. Figure 6(b) shows the measured difference between the TE- and TM-polarized edge emission peak positions ($\lambda_{edge(TE)} - \lambda_{edge(TM)}$) in the EELs and the calculated difference between the heavy-hole/light-hole effective band gaps $\lambda_{e1hh1} - \lambda_{e1lh1}$, as a function of the front-emission peak position. Using photoreflectance measurements, we have independently confirmed that the heavy-hole/light-hole effective-band-gap separation does indeed follow the calculated line. In Fig. 6(b) we find that although $\lambda_{edge(TE)} - \lambda_{edge(TM)}$ based on EL measurements lies (within error bars) on the line representing the calculated $\lambda_{e1hh1} - \lambda_{e1lh1}$ for emission peaks at shorter wavelengths, this agreement worsens progressively towards longer wavelengths. We believe that this discrepancy arises due to the large inhomogeneous broadening, coupled with the following two facts. First, the wave functions describing the heavy-hole states away from the zone center have a small but finite p_z component. Therefore, transitions involving heavy holes at energies higher than the band gap also have a weak TM component, in addition to their strong TE component.[17,24] Second, in the emission process the probability of occupation of a state, which has an approximate Maxwell–Boltzmann-like energy dependence at room temperature, plays an important role. When the emission peaks are at shorter wavelengths due to high Ga concentration in the QW, the strain is small and the light-hole states are close in energy to the heavy-hole states, the latter being lowest in energy. Under these circumstances the light-hole states have sufficient probability of occupation and thereby dominate the TM emission spectrum, and so the peak of the TM emission is close to the light-hole band edge, as expected. However, in moving to longer peak emission wavelengths, which corresponds to increasing In concentration and strain in the QW, $\lambda_{e1hh1} - \lambda_{e1lh1}$ increases (see Fig. 5), thereby reducing the relative probability of occupation of the light-hole states. For instance, using the results of Fig. 5, a shift in the front-emission peak from 633 to 651 nm would result in a calculated drop in the occupation probability of the light-hole states, relative to that of the heavy holes, by a factor of 2. Therefore, as the emission peaks shift to longer

Downloaded 02 Sep 2003 to 158.144.58.158. Redistribution subject to AIP license or copyright, see http://ojps.aip.org/japo/japcr.jsp

wavelengths, the heavy-hole contribution to the TM emission increases with respect to that of the light hole. Here, however, the large inhomogeneous broadening prevents us from distinguishing between these two contributions to the TM polarization (see Fig. 2). What is observed is a shift in the resultant TM emission peak towards the heavy-hole band gap, thereby reducing the difference between the TE and TM emission peak positions, as seen in Fig. 6(b). However, in a situation where inhomogeneous broadening is not significant, so that one can unambiguously determine the light-hole-related peak in the TM-polarized emission, it would then be possible to determine the composition and strain in the QW active region simply by comparing the TE and TM edge-emission spectra.

IV. CONCLUSION

In conclusion, we have shown that edge-emission electroluminescence measurements using ITO-coated glass as transparent electrodes can be very useful for postgrowth nondestructive characterization of VCSELs at room temperature. Although other techniques such as photoreflectance have been shown to work well for VCSELs with lower reflectivity DBRs, with this technique one can easily determine the QW emission spectra as well as the cavity mode in all types of VCSELs. For a more accurate estimate of the QW parameters, a few equivalent EELs are useful to estimate the reabsorption-induced redshifts in the edge-emission spectra. However, if the inhomogeneous broadening is not large, then the QW composition and strain can be determined simply from the separation of the peaks of the two orthogonally polarized edge-emission spectra alone. Although the present measurements were done on visible light-emitting VCSELs, this technique is applicable to VCSELs emitting anywhere in the transparency window of ITO film on glass (typically, $\simeq$400–2000 nm).

ACKNOWLEDGMENTS

The authors acknowledge helpful discussions with A. R. Adams and S. J. Sweeney, and thank S. Pinches and J. Woodhead for providing data on device performance. The financial support of EPSRC-UK and the BREDSELs project of the European Community is also acknowledged. The samples were grown by Epitaxial Products International Ltd.

[1] K. Iga, F. Koyama, and S. Kinoshita, IEEE J. Quantum Electron. **QE-24**, 1845 (1988).
[2] T. E. Sale, *Vertical Cavity Surface Emitting Lasers* (Research Studies, Taunton, 1995).
[3] B. Tell, K. F. Brown-Goebeler, R. E. Leibenguth, F. M. Baez, and Y. H. Lee, Appl. Phys. Lett. **60**, 683 (1992).
[4] G. Hasnain, K. Tai, L. Yang, Y. H. Wang, R. J. Fischer, J. D. Wynn, B. Weir, N. K. Dutta, and A. Y. Cho, IEEE J. Quantum Electron. **QE-27**, 1377 (1991).
[5] C. H. McMahon, J. W. Bae, C. S. Menoni, D. Patel, H. Temkin, P. Brusenbach, and R. Leibenguth, Appl. Phys. Lett. **66**, 2171 (1995).
[6] H. Okamoto, T. Tadokoro, Y. Kondo, and M. Nakao, Jpn. J. Appl. Phys., Part 1 **36**, 5365 (1997).
[7] H. Gebretsadik, K. Kamath, K. K. Linder, X. Zhang, P. Bhattacharya, C. Caneau, and R. Bhat, Appl. Phys. Lett. **71**, 581 (1997).
[8] S. Moneger, H. Qiang, F. H. Pollak, D. L. Mathine, R. Droopad, and G. N. Maracas, Solid State Commun. **39**, 871 (1996).
[9] P. D. Berger, C. Bru, T. Benyattou, G. Guillot, A. Chenevas-Paule, L. Couturier, and P. Grosse, Appl. Phys. Lett. **68**, 4 (1996).
[10] P. J. Klar, G. Rowland, P. J. S. Thomas, A. Onischenko, T. E. Sale, T. J. C. Hosea, and R. Grey, Phys. Rev. B **59**, 2894 (1999).
[11] D. T. Schaafsma and D. H. Christensen, Phys. Rev. B **54**, 14618 (1996).
[12] S. Gramlich, J. Sebastian, M. Weyers, and R. Hey, Phys. Status Solidi A **152**, 293 (1995).
[13] Y. Zhu, D. J. Gauthier, S. E. Morin, Q. Wu, H. J. Carmichael, and T. W. Mossberg, Phys. Rev. Lett. **64**, 2499 (1990).
[14] S. Ghosh and T. J. C. Hosea, Rev. Sci. Instrum. **71**, 1911 (2000).
[15] D. P. Bour, in *Quantum Well Lasers*, edited by P. S. Zory (Academic, New York, 1993).
[16] C. H. Henry, R. A. Logan, H. Temkin, and F. R. Merritt, IEEE J. Quantum Electron. **QE-19**, 941 (1983).
[17] J. Singh, *Physics of Semiconductors and Their Heterostructures* (McGraw-Hill, New York, 1993).
[18] S. Ghosh, B. M. Arora, K. P. Homewood, W. P. Gillin, O. M. Khreis, and K. E. Singer, J. Phys.: Condens. Matter **10**, 9865 (1998).
[19] F. H. Pollak, in *Semiconductors and Semimetals*, edited by T. P. Pearsal (Academic, New York, 1990), Vol. 32.
[20] *Landolt-Bornstein Numerical Data and Functional Relationships in Science and Technology, New Series III*, edited by O. Madelung, W. von der Osten, and U. Rossler (Springer, Berlin, 1982), Vol. 17a.
[21] O. P. Kowalski, J. W. Cockburn, D. J. Mowbray, M. S. Skolnick, R. Teissier, and M. Hopkinson, Appl. Phys. Lett. **66**, 619 (1995).
[22] H. B. Bebb and E. W. Willams, in *Semiconductors and Semimetals*, edited by R. K. Willardson and A. C. Beer (Academic, New York, 1972), Vol. 8.
[23] G. Bastard, *Wavemechanics Applied to Semiconductor Heterostructures* (Halsted, New York, 1988).
[24] J. Y. Marzin, M. N. Charasse, and B. Sermage, Phys. Rev. B **31**, 8298 (1985).

Downloaded 02 Sep 2003 to 158.144.58.158. Redistribution subject to AIP license or copyright, see http://ojps.aip.org/japo/japcr.jsp